

# Inelastic effects in electron transport studied with wave packet propagation.

S. Monturet<sup>1</sup> and N. Lorente<sup>1,2</sup>

<sup>1</sup>*Laboratoire Collisions, Agrégats, Réactivité,*

*UMR5589, Université Paul Sabatier,*

*118 route de Narbonne, 31062 Toulouse cédex, France*

<sup>2</sup>*Centre d'Investigació en Nanociència i Nanotecnologia (CSIC-ICN),*

*Campus de la UAB, 08193 Bellaterra, Spain*

(Dated: November 15, 2018)

## Abstract

A time-dependent approach is used to explore inelastic effects during electron transport through few-level systems. We study a tight-binding chain with one and two sites connected to vibrations. This simple but transparent model gives insight about inelastic effects, their meaning and the approximations currently used to treat them. Our time-dependent approach allows us to trace back the time sequence of vibrational excitation and electronic interference, the vibrationally introduced time delay and the electronic phase shift. We explore a full range of parameters going from weak to strong electron-vibration coupling, from tunneling to contact, from one-vibration description to the need of including all vibrations for a correct description of inelastic effects in transport. We explore the validity of single-site resonant models as well as its extension to more sites via molecular orbitals and the conditions under which multi-orbital, multi-vibrational descriptions cannot be simplified. We explain the physical meaning of the spectral features in the second derivative of the electron current with respect to the bias voltage. This permits us to nuance the meaning of the energy value of dips and peaks. Finally, we show that finite-band effects lead to electron back-scattering off the molecular vibrations in the regime of high-conductance, although the drop in conductance at the vibrational threshold is rather due to the rapid variation of the vibronic density of states.

## I. INTRODUCTION

The importance of inelastic effects in electronic transport in molecular junctions is widely recognized and it is a rich, active research field. Several recent reviews on the topic give a clear idea of its breadth<sup>1,2</sup>. Advanced new experimental techniques show that electrons transport through a few-atom system is strongly dependent on the vibrational degrees of freedom of the system. As miniaturization decreases device sizes, the role of atomic vibrations needs to be considered in the device functionalities. This dependence has been shown to profoundly alter the device behavior: from new channels of conduction<sup>3</sup> to heating of the junction<sup>4</sup>. It is then important to understand the role of inelastic effects and the parameters that control them.

A large body of research has been devoted to inducing controlled inelastic effects. A recent review article<sup>5</sup> shows that inelastic effects in a tunneling junction can be used to chemically analyze the molecules at the junction by inelastic electron tunneling spectroscopy (IETS)<sup>6</sup>, to induce reactions by displacing atoms<sup>7</sup>, and to use molecular conformational changes as a switch for possible devices<sup>8</sup>. In this way, the scanning tunneling microscope (STM) induces the reaction and also detects its product, a dramatic example is the modification and detection of trans-2-butene on Pd (110)<sup>9</sup>. The effect of local vibrations during electron flow has also been revealed in careful experiments of photon analyses<sup>10</sup> yielding an unprecedented insight in vibrational dynamics. Not only has the tunneling junction of an STM been used to explore the coupled electron-vibration dynamics, also point contact spectroscopy has been used in molecular wires<sup>11,12</sup>, where the conductance showed drops at the molecular vibrational onset.

These many experimental results call for important theoretical development. Indeed, the last years have seen several theoretical works spanning most of the experimental systems: from tunneling inelastic spectra<sup>13,14,15</sup> to point contact spectroscopy<sup>16,17,18</sup>, from systematic approaches studying different parameters<sup>19,20</sup> to lowest-order expansion with ab-initio parameters<sup>21,22</sup>. A thorough review on methodology and results can be found in Ref. 2.

A quantitative description of inelastic processes is mandatory in order to assess the relevance of the different ingredients characterizing electron transport on the atomic scale. Recent developments in *ab-initio* calculations together with transport calculations permit us to grasp the essential parameters and, eventually, produce predictive calculations. Yet,

the typical *ab-initio*-based calculations are on the one-hand-side heuristical, because a well established dynamical theory of electron transport is yet to come<sup>23</sup>, and on the other hand-side, they are complex and difficult to interpret. Most *ab-initio* approaches use ground state density functional theory with non-equilibrium Green's functions (NEGF), this combination is not justified, and the results have the full complexity of NEGF. As signaled in Ref. 23, new methodology to treat quantum transport will be probably based in time dependent density functional theory (TDDFT). Recent results show that it is possible to treat nuclear (semiclassically) and electronic (quantally) degrees of freedom within TDDFT to treat the non-adiabatic transport problem<sup>24,25</sup>. New developments go a step further in the treatment of correlated electron-ionic dynamics<sup>26</sup>. But time-dependent methodology can have other benefits beyond its correctness. In particular, it can be used to develop a physical picture of the electron diffusion process, in this way yielding complementary information to the more involved NEGF approach. Time-dependent approaches can also have interesting numerical behavior. Indeed, electron transport treated with the short-iterative Lanczos method<sup>27</sup> has a quasi-linear scaling for sparse Hamiltonians.

In this article, we explore inelastic effects in electron transport by means of electronic wave packet propagations in an idealized atomic-size system. We consider tight-binding chains connected to one and two vibrating electronic sites. These vibrating sites can hold one and two nuclear modes that are coupled to linear order in the nuclear displacement with the electronic degrees of freedom. Despite the simplicity of this model system, the main one-electron ingredients are included, and the time resolved solution permits us to have insight different from the perturbation-theory Green's functions results. Similar treatments have already been performed for the case of electron-molecule collisions<sup>28</sup> and for inelastic effects in transport<sup>29</sup>.

The calculations presented here are distant from the experimental situation because the model system is very simplified and because many-electron problems are absent. Indeed, recent treatments show the richness of effects associated with the many-electron aspects of the problem<sup>30</sup>, as well as the non-equilibrium many-phonon problem<sup>31,32</sup>. Despite, the absence of these very interesting ingredients of inelastic transport, our calculations can help in understanding inelastic effects because there are situations in which one-electron transport is justified even in the presence of inelastic effects<sup>33</sup>. To a certain degree, our calculations are equivalent and complementary to those of H. Ness<sup>34</sup> the main difference being that a

time-dependent approach is adopted in the present study.

## II. TIME-DEPENDENT WAVE PACKET PROPAGATION

Stationary electron transport does not need a time-dependent description. However, insight on vibrational excitation processes during the current flow can be gained by time-dependent calculations. Numerically, a time-dependent description can benefit from the quasi-linear scaling using sparse Hamiltonians. As in stationary descriptions, the bottleneck of the calculation lies in the matrix time vector product of the Hamiltonian acting on a system's vector. Hence, a time-dependent approach can yield especial insight in the actual transport process in a realistic nanoscale system by using a localized basis set that leads to a sparse Hamiltonian. This strategy seems to be particularly appealing for the description of conduction in nanowires<sup>35</sup> and nanotubes<sup>36</sup>. In this section, we explore the general time-dependent methodology using wave packets, beyond the Kubo linear theory of Refs. 35,36.

A particularly interesting time-dependent approach to have information on the full electronic trajectory is the short-iterative Lanczos (SIL) wave packet propagation<sup>27</sup>. The initial-value problem is solved by applying the evolution operator to the initial wave function, so that the solution reads,  $\Psi(t) = e^{-i\mathcal{H}t}\Psi(0)$ , where  $\mathcal{H}$  is the Hamiltonian of the system under consideration (atomic units are used throughout,  $\hbar = m = e = 1$ , unless otherwise specified). The use of this equation is inconvenient in the case of large matrix dimensions because it implies a diagonalisation. Instead, we prefer to use a numerical approximation which consists in successive infinitesimal evolutions of the wave function,  $\Psi(t + \Delta t) = e^{-i\Delta t\mathcal{H}}\Psi(t)$ . In order to have an efficient implementation, the SIL method truncates the Hilbert space to a subspace spanned by a few vectors. The computation of this truncated subspace is the bottleneck of the calculation because the matrix-time-vector product to generate the subspace is performed on the total dimension of the problem. Despite the truncation, the richness of the full Hamiltonian spectrum is recovered by repeating this operation for all the different time steps and propagating in this way the initial wave packet.

Let  $\Phi_1$  be a starting vector, the Lanczos propagation method consists in the construction of a Lanczos matrix following the recursion relation<sup>37,38</sup>,

$$\beta_{j+1}\Phi_{j+1} = \mathcal{H}\Phi_j - \alpha_j\Phi_j - \beta_j\Phi_{j-1}, \quad j \geq 1 \quad (1)$$

where  $\alpha_j$  are the new diagonal matrix elements of the new tridiagonal matrix and  $\beta_j$  are the new upper and lower diagonal matrix elements. Since the recurrence relation is started by  $\Phi_1$ , initial wave function,  $\Psi(t = 0)$ , then  $\beta_1 = 0$  and  $\Phi_0 = 0$ . The vectors  $\Phi_j$  are called Krylov vectors, and define the Krylov space of order  $l$ , by spanning the subspace given by  $\{\Phi_j\}$ , namely

$$\mathcal{K}^l = \text{Span}\{\Phi_1, \mathcal{H}\Phi_1, \dots, \mathcal{H}^{l-1}\Phi_1\}. \quad (2)$$

The Krylov vectors are orthogonal by construction, they may be normalized, and define thus a basis set in which the Hamiltonian can be expressed. In this basis, the Hamiltonian is tridiagonal. Additionally, the order  $l$  can be much lower than the initial matrix dimensions. Consequently, the Lanczos matrix can be easily diagonalized using conventional algorithms. Regarding the Krylov vectors, it is known that for relatively large values of  $l$ , their orthogonality can be lost, this is the reason why we have set sufficiently small time steps to keep a rather small order  $l$  ( $l \leq 9$ ). Its value can be changed at each step in order to optimize the performances of the calculation, lowering the computational cost as  $l$  decreases. An excellent description of this dynamical control of the accuracy of the Lanczos propagation method can be found in Ref. 39.

Another important feature is the undesirable effects provoked by the finite size of the propagation grid. To eliminate artificial reflections of the wave packet at the boundaries, we use a parabolic absorbing potential. In order to account for the errors which may be introduced by the reflections at the boundaries in the presence of the absorbing potential, we calculated the reflection coefficient with a broad wave packet. We found that less than 0.01% of the wave packet was reflected at any energy.

To compute the energy-resolved transmission or reflection coefficients we use the virtual detector technique<sup>40</sup> which consists in the evaluation of the wave function some sites after the region where the electron-vibration interaction takes place. By a time-to-energy Fourier transform, transmission or reflection coefficients are obtained. In the inelastic case, this should be done for each vibrational state of the total wave function. Hence, for a 1-D tight-binding chain, the partial transmission,  $\mathcal{T}_n(\omega)$ , is given by

$$\mathcal{T}_n(\omega) = \frac{|\psi_{d,n}^{int}(\omega)|^2}{|\psi_{d,0}^{bare}(\omega)|^2} \quad (3)$$

where we have assumed zero temperature and an initial wave packet in the vibrational ground state,  $n = 0$ .  $\psi_{d,n}^{int}(\omega)$  is the energy-resolved wave function in the vibrational state  $n$ , after the interacting region. The detector has been located on site  $d$ .  $\psi_{d,0}^{bare}(\omega)$  is the wave function computed with the same virtual detector but considering a bare Hamiltonian containing no vibrational degrees of freedom nor elastic defects.

To analyze quantities such as total transmissions, especially for non-trivial Hamiltonians which may have two or more vibrating electronic states, we have computed the density of states projected on any state, for instance, on any linear combination of the tight-binding states. Consider a state  $|\alpha, n\rangle$ , with  $\alpha$  a particular electronic state and  $n$  its vibrational state, evolving with Hamiltonian  $\mathcal{H}$ . The density of states projected on  $|\alpha, n\rangle$  reads<sup>41</sup>,

$$\rho(\omega) = \int_{-\infty}^{\infty} \frac{dt}{2\pi} e^{i\omega t} \langle \alpha, n | e^{-i\mathcal{H}t} | \alpha, n \rangle. \quad (4)$$

### III. THE PHYSICAL MODEL

The Fröhlich-Holstein model<sup>42</sup> is used to represent the combined electron-vibration system: the electron-vibration coupling is assumed to be linear in the normal-mode coordinates. If we assume only one mode of vibration, and a single site, the Hamiltonian reads,

$$\begin{aligned} \mathcal{H} = & \varepsilon_0 c_0^\dagger c_0 + \sum_{k,i} \varepsilon_{k,i} c_{k,i}^\dagger c_{k,i} + \sum_{k,i} t_{k,i} (c_{k,i}^\dagger c_{k+1,i} + c_{k+1,i}^\dagger c_{k,i}) \\ & + \sum_{k,i} t_{k,i} (c_{k,i}^\dagger c_0 + c_0^\dagger c_{k,i}) + \Omega b^\dagger b + M c_0^\dagger c_0 (b^\dagger + b) \end{aligned} \quad (5)$$

where  $c_k^\dagger$  and  $c_k$  are the fermionic operators which create and annihilate an electron in state  $k$ . Similarly,  $b^\dagger$  and  $b$  are the bosonic operators that create and annihilate a quantum of energy  $\Omega$  in the considered vibrational mode. The first term in the Hamiltonian (6) refers to the site where the interaction takes place, it has an on-site energy of  $\varepsilon_0$ . The second describes the energy of site  $k$  of chain  $i$ . For simplicity we will be dealing with only two chains ( $i = L, R$ : left and right). The third term describes the couplings among sites of chain  $i$ . Here, we just consider nearest neighbours. The fourth term is the coupling between the two semi-infinite chains and the state of energy  $\varepsilon_0$ . The fifth term is the energy of the harmonic oscillator. Finally, the last term describes the electron-phonon interaction. In

this single-state single-mode model,  $M$  is only a scalar which represents the strength of the interaction. It is called the electron-phonon coupling. In the present work, we have explored both an electronic single site coupled to vibrations, and a double site. In the latter case,  $M$  will be a  $2 \times 2$  matrix, as presented in section V.

Using a tensorial product description of the electronic and nuclear coordinates, the full Hamiltonian can be expressed in matrix form:

$$\mathcal{H} = \begin{pmatrix} \mathcal{H}^{(0)} & \hat{M} & 0 & & & & \\ \hat{M} & \mathcal{H}^{(1)} & \sqrt{2}\hat{M} & 0 & & & \\ 0 & \sqrt{2}\hat{M} & \mathcal{H}^{(2)} & \sqrt{3}\hat{M} & 0 & & \\ & 0 & \sqrt{3}\hat{M} & \mathcal{H}^{(3)} & \sqrt{4}\hat{M} & 0 & \\ & & & \ddots & \ddots & \ddots & \\ & & & 0 & \sqrt{N-1}\hat{M} & \mathcal{H}^{(N-1)} & \end{pmatrix} \quad (6)$$

where we have used a block representation in the vibrational basis  $\{|n\rangle\}$ . The diagonal elements are electronic Hamiltonians, which define the propagation of a wave-packet in a vibrational subspace. For clarity we give their tight-binding representation,

$$\mathcal{H}^{(n)} = \begin{pmatrix} \ddots & \ddots & \ddots & & & & \\ 0 & t & n\Omega & t & 0 & & \\ & 0 & t & n\Omega & T_l & 0 & \\ & & 0 & T_l & \varepsilon_0 + n\Omega & T_r & 0 \\ & & & 0 & T_r & n\Omega & t & 0 \\ & & & & 0 & t & n\Omega & t & 0 \\ & & & & & & & \ddots & \ddots & \ddots \end{pmatrix} \quad (7)$$

where  $n$  labels a particular vibrational state in the harmonic approximation. The  $t$  are off-diagonal matrix elements which connect the nearest neighbours sites inside the left and right chain. The  $T_l$  and  $T_r$  play the same role as  $t$ , they connect the chains to the site which has on-site energy  $\varepsilon_0$ . The diagonal term  $n\Omega$  accounts for the energy the electron must exchange with the vibrational degrees of freedom of the system. If it propagates from one vibrational state to another, it must lose or gain  $\Omega$ , the energy quantum of the vibration.

The matrices  $\hat{M}$  in (6) couple the Hamiltonians  $\mathcal{H}^{(n)}$  in the different vibrational subspaces. In the case of a single-site impurity,  $\hat{M}$  is essentially a sparse matrix with the same dimensions

as  $\mathcal{H}^{(n)}$ , where only one single element is non-zero, the one connecting the diagonal matrix elements of energy  $\varepsilon_0 + n\Omega$  and  $\varepsilon_0 + (n+1)\Omega$ . In Hamiltonian (6), the factors that multiply  $\hat{M}$  come from the matrix representation of the bosonic operators, they correspond to the factors which appear in the well known relations  $b^\dagger|n\rangle = \sqrt{n+1}|n+1\rangle$  and  $b|n\rangle = \sqrt{n}|n-1\rangle$ . We note that Hamiltonian (6) is truncated, the number of vibrations that are considered in the calculation is  $N$  in this example. This number  $N$  may be sufficiently large to represent suitably the vibrational space. A detailed study of the convergency of the calculation is presented hereafter.

Let us consider a molecule between two electrodes, modeled by a single state connected to two chains. In this single-site case, Y. Meir and N. S. Wingreen<sup>43</sup> have shown that the current can be expressed as follows,

$$\mathcal{J} = -\frac{1}{\pi} \int [f_L(\omega) - f_R(\omega)] \text{Im}\{\text{tr}[\Gamma G^r]\} d\omega, \quad (8)$$

where  $\Gamma$  is defined as a function of the couplings to the right and left leads,  $\Gamma = \frac{\Gamma_R \Gamma_L}{\Gamma_R + \Gamma_L}$ .  $G^r$  is the retarded green function of the molecule, and  $f_{L(R)}$  is the Fermi distribution of the left (right) lead. This formula applies in the case where the couplings to the leads only differ by a constant factor,  $\lambda$ , such that  $\Gamma_L = \lambda \Gamma_R$ . This is always so in the wide-band limit for the single-site case. This is not the case beyond the wide-band limit.

The equation above can be viewed as the integral of a quantity that we identify as a transmission, multiplied by an energy window given by the difference of the Fermi distributions of the leads, meaning that a current will flow if both the transmission is non-zero and the voltage applied between the electrodes is sufficiently large. Following the derivation by H. Ness<sup>34</sup> at the zero temperature limit, the transmission reads,

$$\text{Im}\{\text{tr}[\Gamma(\omega)G^r(\omega)]\} = \Gamma(\omega)\text{Im}G_{00}^r, \quad (9)$$

where  $G_{00}^r$  is the projection of the Green function in the  $n = 0$  vibrational subspace,  $G_{00}^r = \langle 0|G^r|0\rangle$ . This means that the transmission is related to the projected density of states, Eq. (4), in such a way that, if we consider the wide-band approximation, where the coupling  $\Gamma$  is independent of energy, the transmission is proportional to the density of states projected in the  $n = 0$  subspace. By using the optical theorem one can explicitly retrieve the vibrationally excited states in the inelastic current<sup>34</sup>.

In the case of the wave packet calculation, we can extend these equations for the calculation of the electronic current. We approximate the conductance assuming that the Fermi level only enters to define possible final electronic states (otherwise the calculation is fully one-electron, and in general we will not consider a Fermi level)

$$\sigma(\omega) = \frac{1}{\pi} \sum_n \mathcal{T}_n(\omega) [f_L(\omega + n\Omega) + f_R(n\Omega - \omega)], \quad (10)$$

where the factor  $\frac{1}{\pi}$  is the conductance quantum in atomic units. The terms between brackets are introduced to account for the opening of vibrational channels since they contain the Fermi distribution functions of the left electrode,  $f_L$  and the right one,  $f_R$ , at zero bias voltage in the present case. Actually, when electrons do not have sufficient energy to deposit it into the vibrational degrees of freedom of the system, only the  $\mathcal{T}_0(\omega)$  is to be considered in the conductance. The same holds if the energy of the incident electron is sufficient to excite one vibration, in this case we consider the sum of  $\mathcal{T}_0(\omega)$  and  $\mathcal{T}_1(\omega)$ . Nevertheless, the calculation should be performed with a sufficiently high value of  $n$  in order to take into account the influence of closed channels in the conductance. Finally, the current as a function of the voltage,  $V$ , can be written as the integral over energy of the conductance,

$$\mathcal{J}(V) = \int_{-\infty}^{\infty} \sigma(\omega) [f_L(\omega) - f_R(\omega)] d\omega. \quad (11)$$

The terms between brackets ensures that the transmitted electrons go from occupied states to empty ones where the voltage dependence is included.

The treatment presented here is complementary of the one by H. Ness<sup>34</sup>. Indeed, the physical model is the same one, the difference is the solution method. As in the case of Ref. 34 the present approach is single-electron, neglecting both electron occupation and electron-electron correlation effects.

#### IV. SINGLE-SITE RESONANT MODEL RESULTS

Let us assume a single state coupled to the two 1-D tight-binding chains of the above model. Figure 1 shows the results of a wave packet propagation. Figure 1 (a) is the elastic wave packet,  $n = 0$ , because we assume that no vibration is initially excited in the system and the temperature is zero. The present system is two 1-D electrodes symmetrically coupled to

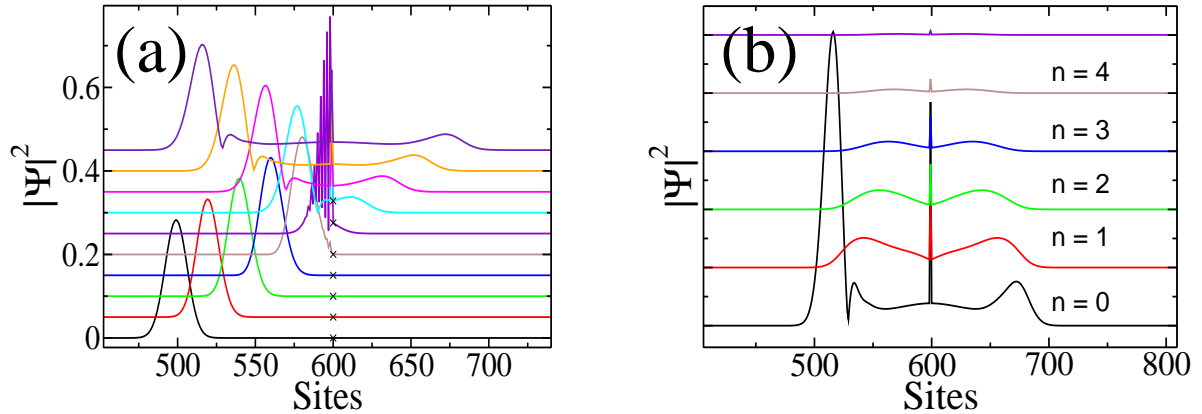


FIG. 1: (Color online) (a) Spatial dependence for the squared modulus of the electronic wave function at different times, arbitrarily shifted for representation purposes. Case (a) is the elastic propagation of the wave packet,  $n = 0$ , where  $n$  is the vibrational quantum number. Symmetric hopping matrix elements,  $T_L = T_R$  have been used. In (b) the wave packet is represented at the same instant in time for different vibrational states  $n$ . The wave packet is initially propagated from the left electrode in the vibrational ground state,  $n = 0$ . The calculations are performed at zero temperature. When the wave packet starts populating the site number 600 (marked with a cross in (a)), the different vibrational states are populated (b), and the vibrationally excited wave packet starts propagating in both directions, indistinctly, due to the symmetric electronic couplings.

the vibrating site. Hence, in Fig. 1 (b) we see that only the reflected wave packet is different from the transmitted one in the elastic channel,  $n = 0$ , while it is identical for the inelastic channels: the electron reaches the active site and populates the ladder of excited vibrational states. In each state the electron has a finite and identical left and right transmission.

A simple-minded picture of the structure appearing in the transmission as a function of incident electron energy could be that there is a series of  $N$  resonances displaced by the phonon energy, in agreement with the scheme of Fig. 2. At a given initial electron energy, the wave packet probes the resonant electron site if the energy is within  $n\Omega$  of the resonant site energy. The results is a series of equidistant peaks spaced by  $\Omega$ . This is plotted in Fig. 3 (a). There, the transmission for the single electronic state without electron-vibration coupling is depicted in a dotted line, and the full line corresponds to the case when the electron-vibration coupling is included.

However, the physical picture is more complex than just a series of equidistant reso-

nances. In order to understand the appearance of the vibrational sidebands we divide the transmission according to the final state of the vibrator, Fig. 3 (b). This yields information on the vibrational state once the wave packet has propagated through the resonant site. The result is that each transmission curve for a well-defined final vibrator state displays a similarly rich peak structure. The above picture, Fig. 2, has to be changed: there are complex vibrational pathways, in which different vibrational states are probed before the system is left in a singly well-defined vibrational state. Given the coherence of the electron propagation, the different pathways can interfere and will give rise to Fano lineshapes in the transmission function<sup>52</sup>.

### A. Vibrational state population sequence: electron coherence

Wavepacket dynamics can probe the different structures appearing in the transmission function in order to yield information on the actual interference process. Let us take a vibrational ground state, broad electronic wave packet energetically centered about the first maximum of the full transmission function, Fig. 3. A spatially broad wave packet is almost a planewave and synonymous of a monochromatic packet, hence we can be sure to probe only the structure of the first maximum.

Figure 4 shows the modulus square of the electronic wave function for the first three vibrational levels on the vibrating site as a function of time. We first notice that the population of the vibrations are sequential: the peaks are slightly shifted in time as  $n$  increases. The linear electron-vibration coupling forces this sequential population since  $n$  is changed in steps of one quantum of vibration, Eq. (6). The populations show a time modulation, in the present case, we see that the modulation frequency of the  $n = 1$  wave packet is roughly twice the modulation of the ground state and of  $n = 2$ . This is easily explained by considering populating and depopulating the  $n = 1$  level by populating the  $n = 0$  and the  $n = 2$ . After a certain time the  $n = 2$  level can depopulate again in the  $n = 1$  as well as the  $n = 0$ . Despite the simplicity of the electron-vibration coupling and the electronic model, the final population dynamics depend on the wave packet energy, the strength of the vibrational coupling and the electron lifetime at the site, leading to non-trivial dynamics. The lifetime of the site is fixed by the hopping matrix elements  $T_l$  and  $T_r$ , Eq. (7).

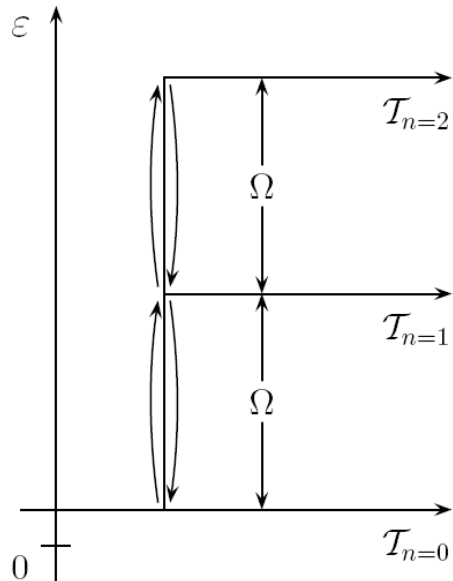


FIG. 2: Vibrational energy level scheme: The electronic wave packet propagates from left to right in the  $n = 0$  vibrational ground state. When the electron wave packet populates the impurity site connected to the vibrator, the population of  $n = 1, n = 2, \dots$ , becomes different from zero and the wave packet propagates in both directions. The transmitted wave packet permits us to compute the transmission resolved in  $n$ . The transmitted wave packet can be assigned to a vibrational channel. The  $n = 0$  channel is the elastic one, that can have contributions from all channels due to the excitation and de-excitation of the vibration during the wave packet propagation. This leads to a rich vibronic structure in the electron transmission even for the elastic channel.

The Fano profile characterizing the transmission functions, Fig. 3, can then be explained by the interference of several of these vibrational pathways. Indeed, asymmetric Fano profiles are the rule in Fig. 3 (b). For the case of the total transmission, the addition over final vibrational states smear out the different profiles, rendering more difficult the determination of an asymmetric Fano profile in the peak sequence.

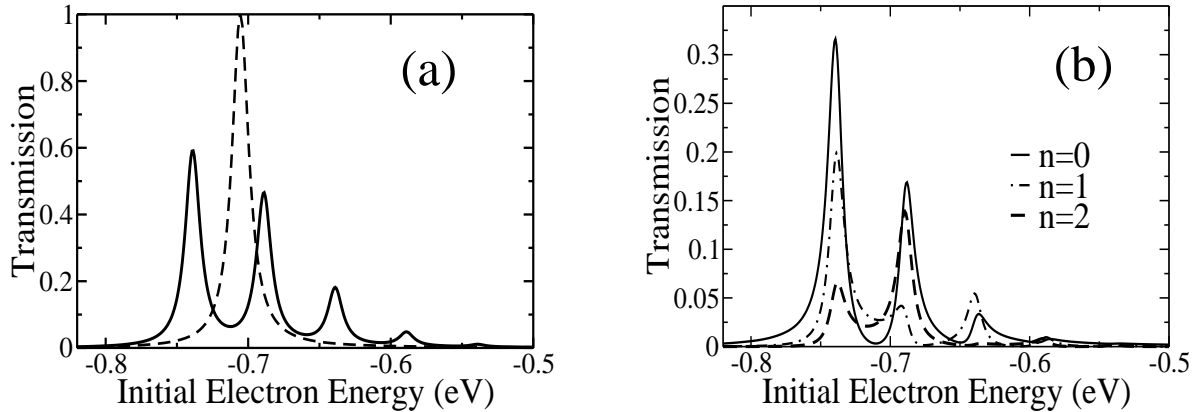


FIG. 3: (a) Electron transmission for two 1-D tight-binding electrodes connected by a single electronic site with electron-vibration coupling (full line) and in its absence (dashed line). (b) Transmission decomposition in the final vibrational state of the single site,  $n$  is the number of vibrational quanta. The elastic transmission is the  $n = 0$  curve in (b). The initial state  $\varepsilon_0 = -0.7$  eV,  $\hbar\Omega = 0.05$  eV, the electron-vibration coupling is  $M = 0.04$  eV and the resonance width is set by the hopping matrix elements  $T_l = T_r = 0.05$  eV. The bandwidth is 2 eV.

### B. Time delay and phase shifts

Spatially narrow wave packets contain most of the energy components needed to span the spectral region of interest, i. e. the main peaks of Fig. 3. The Fourier coefficients in the energy domain can be evaluated to obtain the phase of each component and hence the phase shift between Fourier components. The derivative of the phase shift with respect to energy yields the time delay of the Fourier component in the wave packet<sup>28</sup>. Hence, we can analyze the effect of the vibrational excitation of the electronic site by means of the time delay imposed on the propagating wave packet.

Figure 5(a) shows the phase shift for the elastic component of the wave packet (the  $n = 0$  component). The full phase shift over all of the vibronic peaks is  $\pi$ , this is the phase shift of the electronic resonance. The phase shift of each individual contribution to the transmission is more complex. We see that the phase shift varies rapidly after each maximum, very much indicating a suite of Breit-Wigner-like resonances. Indeed, the phase shift  $\delta$  for a Breit-Wigner resonance of FWHM  $\Gamma$  centered at  $E_0$  is given by<sup>28</sup>:

$$\delta = -\tan^{-1} \left( \frac{\Gamma}{2(E - E_0)} \right).$$

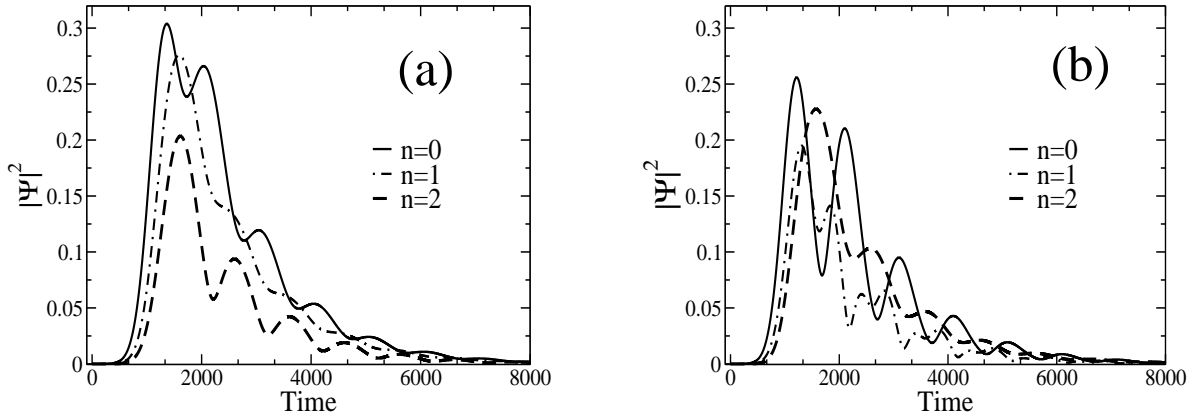


FIG. 4: Time dependence for the squared modulus of the electronic wave function at the site connected to the vibrator. In case (a) an almost monochromatic wave packet has been centered at the energy of the lowest peak of Fig. 3 (b). In the case (b) the wave packet has been centered at the second peak, where the transmission in  $n = 1$  is smaller than the transmission in  $n = 2$ .

The time delay,  $\tau$ , is given by the energy derivative<sup>28</sup> of the phase  $\delta$ :

$$\tau = \frac{d\delta}{dE}.$$

In the case of a single Breit-Wigner resonance, the time delay is then

$$\tau = \frac{\Gamma/2}{(E - E_0)^2 + (\Gamma/2)^2}.$$

On resonance the time delay is just  $\tau = 2/\Gamma$ , yielding direct information on the resonance width,  $\Gamma$ . In the present case, the time delay, Fig. 5(b), gives some definite interpretation: the time delay is maximum once the wave packet has encompassed one of the vibronic resonances. Hence, just above the resonance, the electron is deterred in its propagation by interaction with the vibration. The vibration contributes to the partial width of the electronic resonance, however the total width is independent of the vibration<sup>47</sup>. A spatially narrow wave packet, will have the phase shift and time delay of an electronic resonance regardless of the existence or not of the vibrations. We also find negative time-delays, that correspond to drops in the phase shift. Electrons can hence be expelled from the resonance more easily in the presence of vibrations at certain incident energies. This behavior is due to the interference between two consecutive vibronic resonances. As emphasized in Ref. 28, the time delay has to be interpreted with care in the case of a multichannel problem such

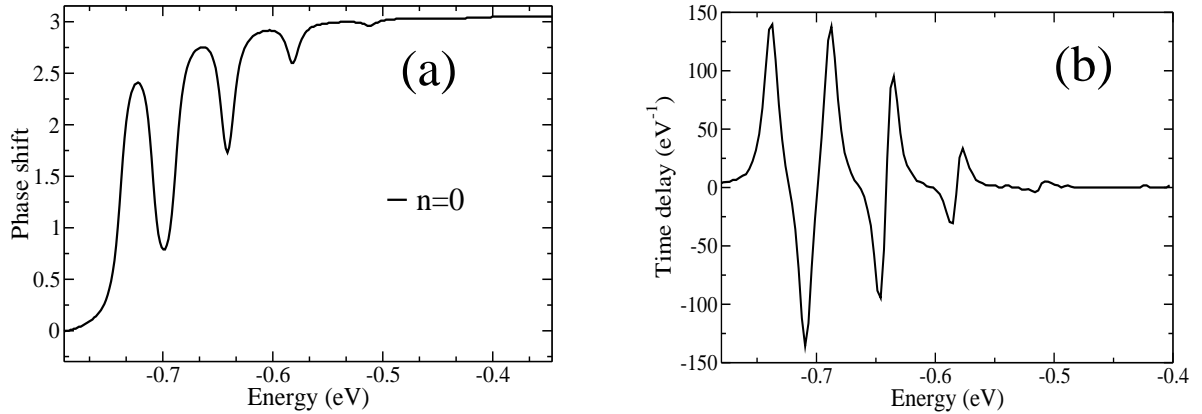


FIG. 5: Electronic phase shift (a) and time delay (b) for the elastic channel,  $n = 0$ , for the case of Fig. 3 (b). The phase shift over the full resonant structure amounts to  $\pi$ , but the vibrational substructure leads to fast variations of the phase, showing the resonant nature of the vibronic peaks of Fig. 3. The time delay is maximum away from each resonance, but it can change signs on resonance, depending on the order of the vibronic peak. This delay/acceleration process is related to the interference path inside the vibrator.

as the present one. The time dependence is indeed complex and the time delay is just a number that cannot summarize the full interference pattern.

The interferences among vibrational paths are ubiquitous in all present results. Their effects can be seen in the Fano-like lineshapes of the transmission function Fig. 3, in the oscillating population of vibrational states with time, Fig. 4 and in the rapid changes of the phase shifts and in the negative time delays, Fig. 5.

### C. Time scales

To develop an understanding of the vibrational excitation process, many authors resort to comparing the different timescales in play<sup>1,2,53</sup>. This is a very appealing approach because it permits us to rationalize the excitation process and the excitation regime of different systems.

Let us define  $\tau_{\text{mol}}$  as the lifetime of an electron in the molecule, which is given by the inverse of the resonance width,  $1/\Gamma$ . Typically, for chemisorbed molecules,  $\Gamma \sim 1 - 3$  eV, which means electron lifetimes in the sub-femtosecond range. In order to estimate the

change in conductance due to an inelastic process, we can compute the inelastic fraction of electrons passing by the molecule. This can be estimated by computing the ratio of the excitation time to the first quantum of vibration,  $\tau_{n=1}$ , and the lifetime of the electron in the molecule,  $\tau_{\text{mol}}$ . Let us estimate the magnitude of the electron-vibration coupling,  $M$ , to attain a measurable change in conductance (larger than 1%). This is the regime where perturbation theory is valid. In this case, the excitation process has been classified as sudden in the electron-molecule collisions literature<sup>54</sup>.

In a sudden process, the molecule is assumed to be very briefly in its negative ion potential energy surface (PES). This can be indeed very brief as has been said above. As in Ref. 3, let us assume that the PES is basically parabolic, but displaced with respect to the neutral PES<sup>56</sup>:

$$E_- = \frac{1}{2}K(Q - Q_-)^2 \quad (12)$$

where  $K$  is the spring constant of the PES related to the mode frequency by  $K = \mu\Omega^2$  where  $\mu$  is some reduced mass (this is easily generalized to the case of multinuclear modes). Here,  $Q_-$  is the displaced center of the negative PES. When the electron flows through the molecule, the molecule is suddenly in its negative PES. Hence, the nuclei experience a force given by

$$F = -\left.\frac{\partial E_-}{\partial Q}\right|_{Q=0}.$$

Then, they acquire a speed,  $v$ , of the order of

$$v \approx -\left.\frac{1}{\mu}\frac{\partial E_-}{\partial Q}\right|_{Q=0} \times \tau_{\text{mol}}$$

and  $\tau_{\text{mol}} \approx 1/\Gamma$ . Hence,

$$v \approx \frac{KQ_-}{\mu\Gamma},$$

where  $KQ_-$  is the electron-vibration linear coupling,  $M/\delta Q_{rms}$  of Eq. (6) with  $\delta Q_{rms} = 1/\sqrt{2\mu\Omega}$  coming from the second quantization of the displacement  $Q$ . The speed gained by the nuclei at an excitation of one quantum of vibration near  $Q = 0$  is  $v_M = \sqrt{2\Omega/\mu}$ . In this way, we find an upper limit for  $\Gamma$ :

$$\Gamma \leq |M|. \quad (13)$$

This simple estimation shows that for strong electron-vibration coupling, vibrational excitation is unavoidable, where strong means larger than the molecule-electrode coupling.

Weak coupling is then the regime when  $|M| \ll \Gamma$ . We can use Fermi's golden rule to estimate the vibrational excitation rate<sup>55</sup>:

$$\frac{1}{\tau_{n=1}} \approx 4 \frac{|M|^2}{\Gamma}.$$

Assuming typical IETS branching ratios  $\tau_{\text{mol}}/\tau_{n=1} \approx 10^{-2}$ , leads to

$$\frac{|M|^2}{\Gamma^2} \leq \frac{1}{400},$$

therefore the coupling becomes  $|M| \sim \Gamma/200$ . For chemisorbed molecules this is in the range of 0.01 eV. This coupling is easily found in a large class of molecules, and therefore IETS is a feasible spectroscopy. This is a simple estimation showing that rather small  $M$  ( $\approx 0.01$  eV) can have a measurable change in conductance for molecules adsorbed on metallic leads.

One more time scale is fixed by the vibrational frequency,  $\Omega$ . As discussed in Ref. 28, there are three basic regimes that can be distinguished:

1.  $\Gamma \ll \Omega$  the negative ion is long lived and the molecule can vibrate in the new state,
2.  $\Gamma \gg \Omega$  the negative ion is short lived and we are in the above sudden regime,
3.  $\Gamma \approx \Omega$  strong interference effects appear due to the nuclear motion.

The time scale given by  $\Omega$ , defines then the type of electron-vibration interaction that will result. In the first case, the electron has ample time to interact with all the nuclear degrees of freedom and depending on the electron-vibration coupling,  $M$ , vibronic signatures can appear. This has been shown in the case of STM studies of electronic states on surfaces<sup>3,57</sup> with a band gap leading to small  $\Gamma$ . The second case corresponds to the IETS case discussed above. The third case has been studied in the gas phase (see for example Ref. 28) but we are not aware of any report on the consequent *boomerang* effect in the electron transport regime.

#### D. Finite-band effects

The wide-band approximation simplifies the expression for the transmission that becomes analytical<sup>47</sup>. One of the results of the wide-band approximation is that the transmission

function and the spectral function or PDOS, Eq. (4), have the same behavior with the electron energy. This is definitely not the case when finite-band effects are considered, indeed, the energy dependence of the coupling to the electrodes leads the transmission function to have a different energy behavior than the site spectral function, Eq. (9). When the initial level,  $\varepsilon_0$  is near the center of the band, the conditions for the wide-band limit are easily attained. As the level approaches one of the band edges,  $\Gamma$  becomes strongly dependent of energy as well as the center of the transmission distribution, Fig. 3.

One of the apparent features is that the transmission peaks become thinner and better defined. As  $\varepsilon_0$  approaches the band edge, many inelastic channels start closing because the final electron energy falls out of the electron band, leading to a substantial decrease in the transmission peaks. This is clearly seen in Fig. 6. The parameters of the transmission calculated in Fig. 6 are exactly the same as for Fig. 3 (a) except that  $\varepsilon_0$  is -0.95 eV instead of -0.7 eV. The bottom of the band is at -1 eV and the quantum of vibration is  $\hbar\Omega = 0.05$  eV. The singular aspect of the peaks is enhanced by the 1-D character of the electrodes. Indeed, when the final energy of the electron approaches the bottom of the band a van Hove singularity appears in the density of states making the transmission more singular. In more realistic cases with 3-D electrodes we expect less singular transmission peaks.

For an electron resonance approaching the top of the band, the situation is rather different. Here, the higher vibronic side bands disappear but the  $n$  convergency remains the same because no channel is closed, leading to low-energy side bands of the same width as for the case of the resonance at the center of the band.

### E. The dynamical polaron shift

The polaron shift is defined as the energy displacement of the first peak in Fig. 3 (a) with respect to the dashed-line peak. The polaron shift is related to the appearance of a vibronic structure. As we showed above, in the time-scale discussion, 2 conditions need be satisfied. Namely,  $M$  must be sizeable and  $\Gamma \ll \Omega$ . This leads to considering<sup>30</sup> the parameter  $p = M^2/(\Gamma\Omega)$ . When  $p > 1$  the polaron shift becomes measurable.

Hyldgaard et al.<sup>30</sup> show that the polaron shift critically depends on the initial occupation of the vibrating electron site. When the electron site is occupied, the transmission function shows a main peak displaced by  $-3M^2/\Omega$ . At half-filling the displacement is  $-2M^2/\Omega$  and

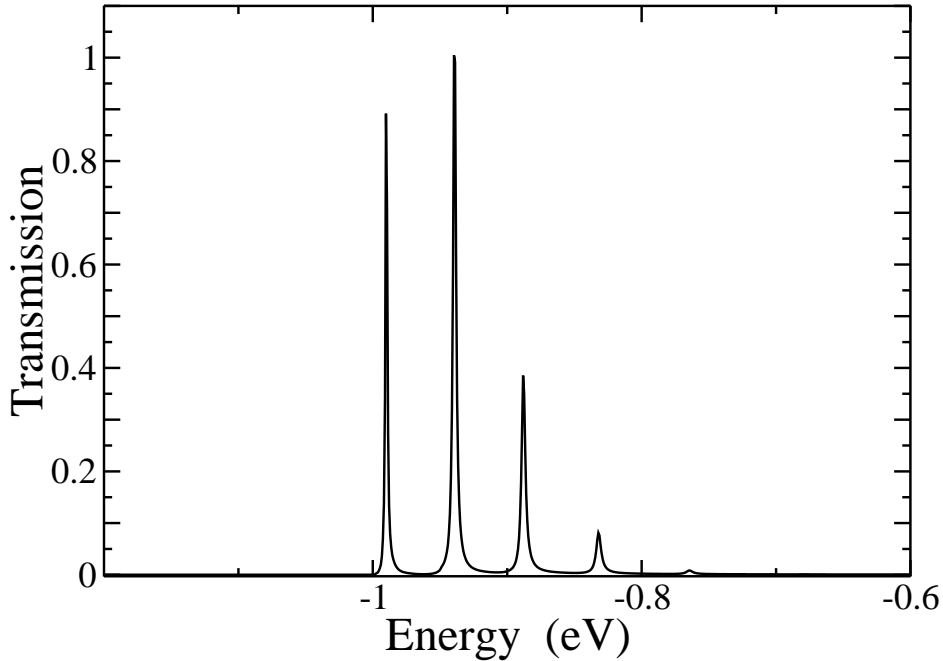


FIG. 6: Transmission function for the same system of Fig. 3 where  $\varepsilon_0$  is -0.95 eV instead of -0.7 eV. The closing of channels due to the band edge leads to sharper and singular-like transmission peaks. The band edge is at -1.0 eV.

for an empty site the polaron shift is  $-M^2/\Omega$ .

We can give a direct interpretation of the polaron shift by using the above parabolic model, Eq. (12). Following the above discussion, the polaron shift for the empty site is  $-M^2/\Omega$  which is equal to  $-\frac{1}{2}KQ_-^2$ . The neutral PES is given by  $\frac{1}{2}KQ^2$ , hence the polaron shift is exactly the energy difference between the neutral PES and the negative one at the nuclear coordinate at which electron capture takes place. Hence, the polaron shift is the energy gain in the formation of the negative intermediate because the electron-vibration coupling permits the electron to probe the negative ion PES. In the absence of coupling, the nuclear coordinates do not evolve, and the negative ion resonance is just a simple lorentzian.

In order to probe the polaron peak, the nuclear wavefunctions in the two ground states (neutral and negative) need to overlap. The overlap is large at weak electron-vibration coupling, hence a well-defined peak appears, just shifted by the energy gain. As the coupling increases, the overlap diminishes, leading to a decrease of the polaron peak. In the limit of strong coupling, the polaron peak is basically zero and a rich structure of evenly distributed peaks of the negative-ion vibrational states is apparent, with a gaussian envelop<sup>57,58</sup>.

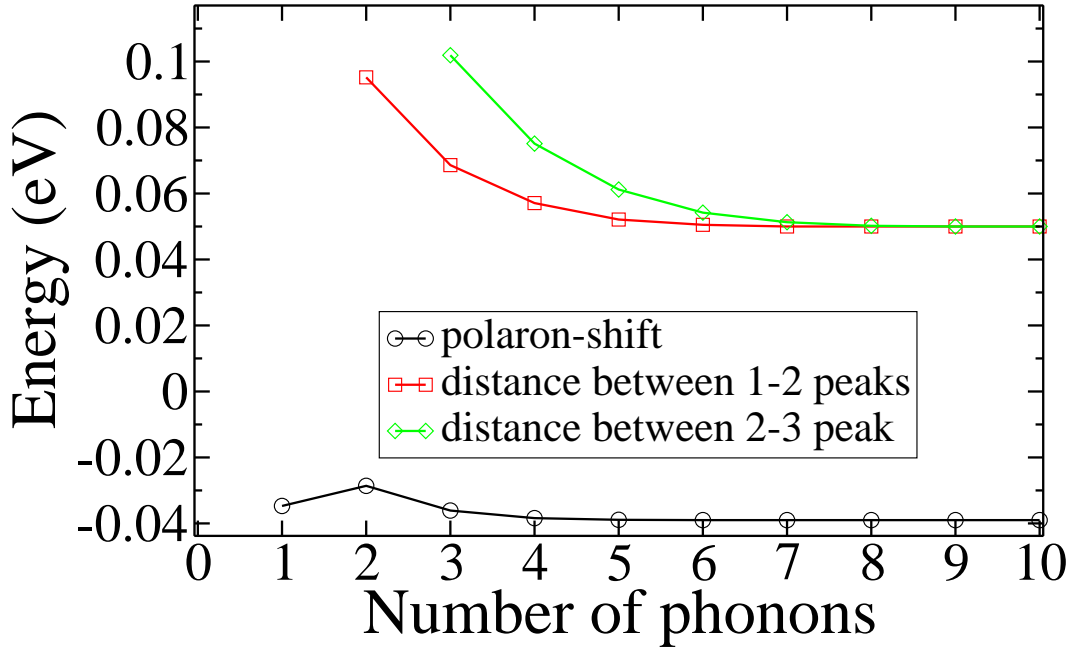


FIG. 7: (Color online) Convergency in the polaron shift and inter-peak distance with the number of vibrational states included in the calculation. The polaron shift is the displacement of the first peak with respect to the resonance without electron-vibration coupling, dashed lines in Fig. 3 (a). It is a critical measurement of the strength of the electron-vibration coupling, and hence, sensitive to convergency. Also sensitive is the inter-peak distance that is equal to  $\Omega$ .

The polaron shift is a good test for the convergency of numerical calculations with the number of vibrational states included in the expansion of Eq. (6). Figure 7 shows the convergency of the polaron shift with the number  $N$  of phonons included in the calculation. A correct value is obtained ( $\approx -0.038eV$ ) at about  $N=5$  phonons. Following the results of the calculation of Hyldgaard et al. for an empty state, the polaron shift would be  $-0.032eV$  with our parameters ( $M = 0.04eV, \Omega = 0.05eV$ )

We also show in Fig. 7 the inter-peak distance as a relevant quantity regarding the convergency of the calculation. We observe that the peaks of lower energy tend to converge with less phonons than the peaks of higher energy, which need a higher number of phonons to be placed at  $\Omega$  the one with respect to the other. Trivially, higher-order peaks need higher  $n$ , otherwise the peak may not even appear in the calculation.

The polaron shift is also very sensitive to the different approximations that are used when evaluating inelastic effects in electron transport. Indeed, the self-consistent Born

approximation (SCBA)<sup>30</sup> yields wrong polaron shifts. Such a study is performed in 34. There, it is shown that the SCBA is equivalent to neglecting the  $\sqrt{n}$  factors of Eq. (6), this leads to wrong interpeak distances. Nevertheless, the SCBA captures much of the physics of inelastic processes and is an all-order theory, becoming reliable enough and very interesting for the evaluation of inelastic processes in a wide range of problems. In the particular case of weak electron-vibration coupling,  $n \approx 1$  and the SCBA is virtually exact.

## V. TWO-SITE RESONANT MODEL RESULTS

Most of the literature devoted to transport in the presence of electron-vibration coupling is based on the single-site model. However, Bringer et al.<sup>29</sup> showed that the single-site case has a behavior that cannot be extended to more realistic systems in which several electronic states are coupled with vibrations. Here, we will analyze when one can reduce the problem to the single-site case and when not. In the same way, we will show that when several vibrations are involved, the neglect of some of the vibrations can lead to qualitatively wrong results.

### A. Two-sites and one vibration

Our previous one-site model is extended to have two electronic sites connected to a vibration. This model has been recently explored in the context of ab-initio based calculations of inelastic transport between two pyramidal electrodes<sup>59</sup>. The simplified two-site model permits us to understand the more complex ab-initio results. The model is given again by Hamiltonian (6) and (6) where  $\varepsilon_0$  and  $M$  are  $2 \times 2$  matrices.

Here, one only vibration is assumed to interact with the electron flow. In the case of weak coupling<sup>59</sup>, this assumption is justified because Eq. (6) is truncated to the first phonon of each mode and the inelastic effects of each mode are separable. In the next section, we will see that when convergency in the number of phonons needs more than one excited vibration, all of the vibrations need to be considered at once.

In this one-dimensional model, there are two only possible modes<sup>59</sup>. We will call them the center-of-mass mode (CM), and the anti-bond-length mode (ABL). The CM mode means that both sites displace in phase, hence the electron-vibration coupling matrix have non-zero

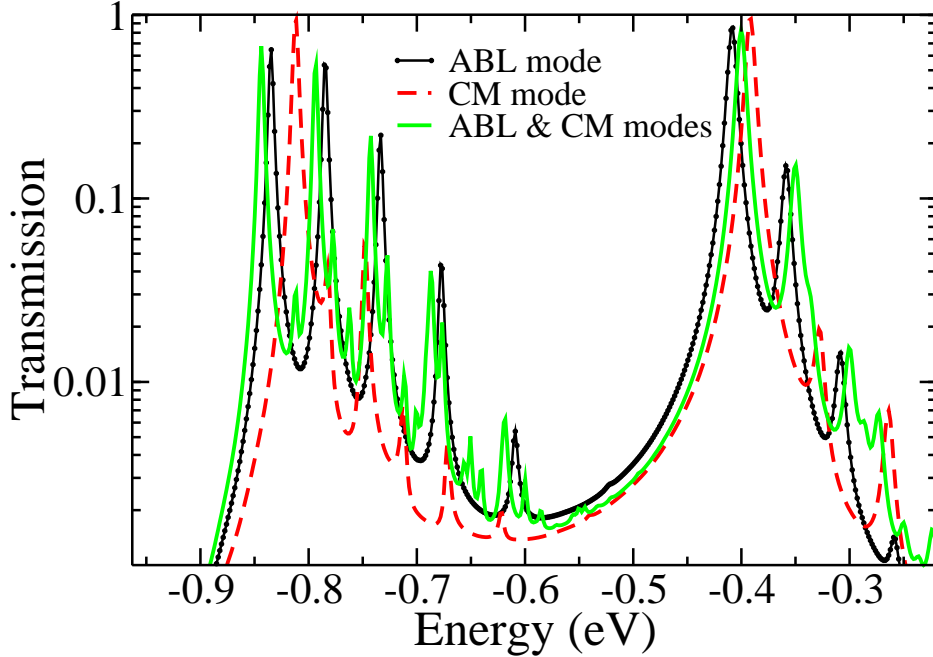


FIG. 8: (Color online) Electron transmission as a function of incident energy for the two-site problem in semilog scale. Two different modes are considered, the anti-bond-length modes (ABL) in full line with dots, and the center-of-mass mode (CM) in dashed lines. These two calculations are performed independently, however when both modes are simultaneously considered the transmission function is different and becomes the full line marked by ABL & CM modes. We see that no direct assignments of the transmission peaks can be performed and the vibronic structure grows in complexity beyond a superposition of transmission peaks from both modes.

onsite elements (the diagonal):

$$\mathbf{M}_{CM} = \begin{bmatrix} m_3 & 0 \\ 0 & -m_3 \end{bmatrix}, \quad (14)$$

and the second element is negative in order to account for the sign of the displacement of each site. In the ABL mode, the sites are moving out of phase, corresponding to an internal stretch mode. Hence, the electron-vibration matrix becomes

$$\mathbf{M}_{ABL} = \begin{bmatrix} m_1 & m_2 \\ m_2 & m_1 \end{bmatrix}. \quad (15)$$

Figure 8 shows the transmission for the ABL and CM modes, independently computed

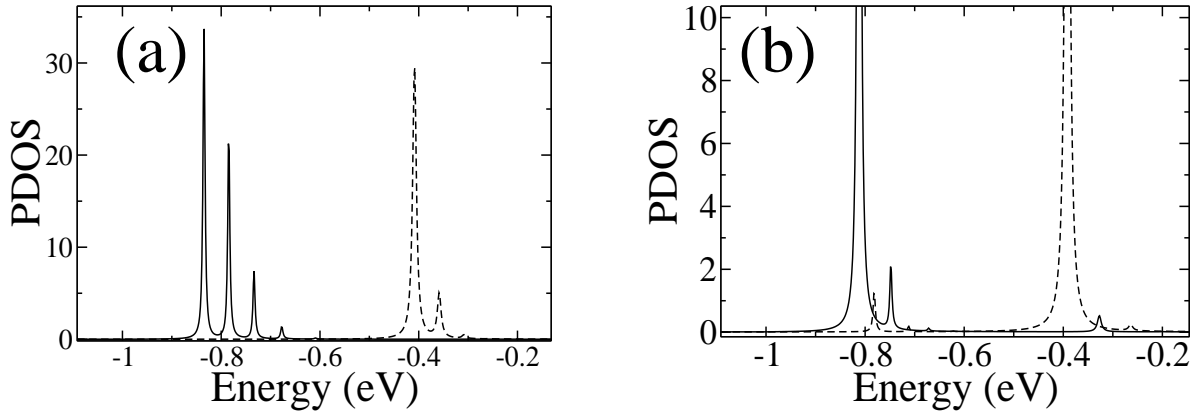


FIG. 9: Projected density of states (PDOS) on molecular orbitals: bonding ( $\sigma$ ) in full line and antibonding ( $\sigma^*$ ) in dashed lines. The modes are considered separately in order to analyze the transmission functions of the ABL mode (full line with dots in Fig. 8) and of the CM mode (dashed line in Fig. 8). In (a) the vibronic density of states for the ABL mode is projected onto the two molecular orbitals and in (b) the vibronic density of states of the CM mode. In (a) we see two distinct series of vibronic peaks corresponding to the bonding and the antibonding molecular orbitals since the ABL mode does not couple these molecular orbitals. However (b) shows mixed structure due to the coupling of molecular orbitals by the CM mode.

and together (to be analyzed in the next section). These figures show series of vibronic peaks difficult to analyze.

In order to analyze the electron transmission, Fig. 8, it is more convenient to use projected density of states (PDOS) of the full vibronic structure on molecular orbitals, Fig. 9(a) for the ABL mode and (b) CM mode. These orbitals are linear combinations of the two sites:

$$|\sigma\rangle = \sqrt{\frac{1}{2}}(|L\rangle + |R\rangle)$$

and

$$|\sigma^*\rangle = \sqrt{\frac{1}{2}}(|L\rangle - |R\rangle)$$

that diagonalize the uncoupled two-site Hamiltonian with eigenvalues  $\varepsilon_0 - t_{\text{mol}}$  and  $\varepsilon_0 + t_{\text{mol}}$ , respectively, where  $\varepsilon_0$  is the level energy for each site and  $t_{\text{mol}}$  is the hopping matrix element between sites.

In this new basis set, the above coupling matrices, Eq. (14) and (15), become:

$$\mathbf{M}_{CM} = \begin{bmatrix} 0 & m_3 \\ m_3 & 0 \end{bmatrix}, \quad (16)$$

and

$$\mathbf{M}_{ABL} = \begin{bmatrix} m_1 + m_2 & 0 \\ 0 & m_1 - m_2 \end{bmatrix}. \quad (17)$$

that hint at the interpretation of the above vibronic peaks. In the case of the CM mode, the  $\sigma^*$  and  $\sigma$  orbitals are coupled via the vibration, while in the ABL case, the molecular orbitals are not mixed by the electron-vibration interaction. This case can then be interpreted as two single-sites connected to a vibration, and hence two vibronic sequences are associated with the spectral feature of  $\sigma^*$  at and the spectral feature of  $\sigma$  at . Since, the effective electron vibration coupling is  $m_1 + m_2$  for  $\sigma$ , the number of peaks and the general vibronic sequence corresponds to stronger coupling than the vibronic sequence of the  $\sigma^*$  peak. This is clearly seen in the PDOS on  $\sigma^*$  and  $\sigma$ , Fig. 9, where we see that the vibronic sequences with  $\sigma^*$  and  $\sigma$  character are energetically localized near the original molecular-orbital peaks.

The CM mode mixes  $\sigma^*$  and  $\sigma$ , hence we obtain vibronic peaks that are shared in the PDOS over both molecular orbitals.

For small enough couplings, we can estimate the vibronic structure keeping just  $n = 1$  in the vibrational part. Hence we can diagonalize Hamiltonian (6) for the sites connected to the vibrations. This can also be expressed by a hybridization scheme, Fig. (10). We realize that the new peaks correspond one-to-one to the peaks found in the PDOS, and that they have contributions in different ratio from the  $\sigma^*$  and  $\sigma$  orbitals according to the matrix elements of  $\mathbf{M}$ . Depending on the magnitude of  $g_M = (\frac{m_3}{\Omega_{CM}})^2$  more or less phonons,  $n$ , will be needed to converge the vibronic sequence<sup>58</sup>, and more or less elements will be included in scheme (10). In order to obtain the type of diagram (a) or (b), only knowledge of the symmetry of the system is required.

In the present case, while the CM mode mixes  $\sigma^*$  and  $\sigma$  orbitals efficiently, the ABL mode does not mix them. Hence, only this last case can be understood by a single-level model.

It is interesting to study the time dependence of the electron occupation of both sites depending on the considered mode. Given the “shuttle-like” motion of the CM mode, one could expect that both sites populate at the same time when they approach together the left electrode and then depopulate when they approach the right electrode. On the other

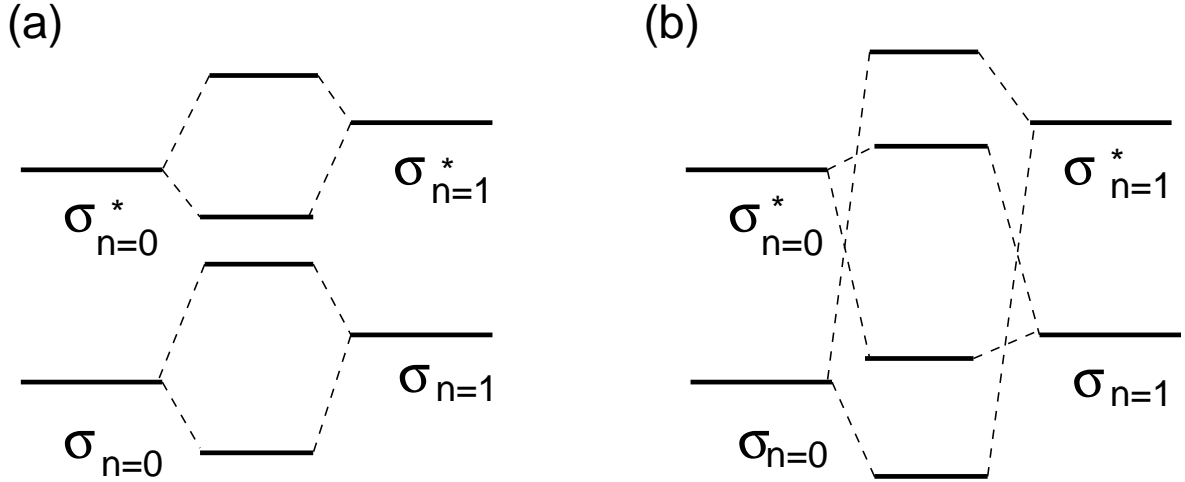


FIG. 10: Hybridization scheme for ABL mode (a) and for CM mode (b) considering only the two first vibrational levels  $n = 0$  and  $n = 1$ . The levels on the left and right are without electron-vibration coupling, but the right levels are shifted by one quantum of vibration with respect to the left levels. The coupled orbitals have a different vibrational state  $n$  because they are mixed by the electron-phonon interaction. It is clearly seen that in the ABL case, the coupling does not mix the molecular orbitals between them ( $\sigma_{n=0}-\sigma_{n=1}$ ,  $\sigma_{n=0}^*-\sigma_{n=1}^*$ ), while in the CM case, the orbitals are mixed ( $\sigma_{n=0}-\sigma_{n=1}^*$ ,  $\sigma_{n=0}^*-\sigma_{n=1}$ ).

hand, the ABL motion is a stretch mode and hence, one site would populate while the other one depopulates.

However, in Fig. 11 (a) we see that the ABL mode leads to population of both sites at the same time, while in presence of the CM mode, Fig. 11 (b), the population sequence is shifted and dependent on time. In this case, the wave packet has been centered about the energy  $\varepsilon_\sigma$  and its energy span is smaller than the difference between  $\varepsilon_{\sigma^*}$  and  $\varepsilon_\sigma$ . The reason for this behavior is that one should think in terms of molecular orbitals rather than site orbitals. In this case, the ABL motion does not couple the  $\sigma^*$  and  $\sigma$  orbitals, hence, the electron populates one of the molecular orbitals,  $\sigma^*$ , at one time and interacts with the vibration in the same way as in the case of the single site. Instead of a single site, we have a single level, otherwise there is no physical difference. Let us approximate the wave packet by the evolution on the two sites:

$$|\Psi(t)_{\text{ABL}}|^2 \approx |\psi_\sigma|^2$$

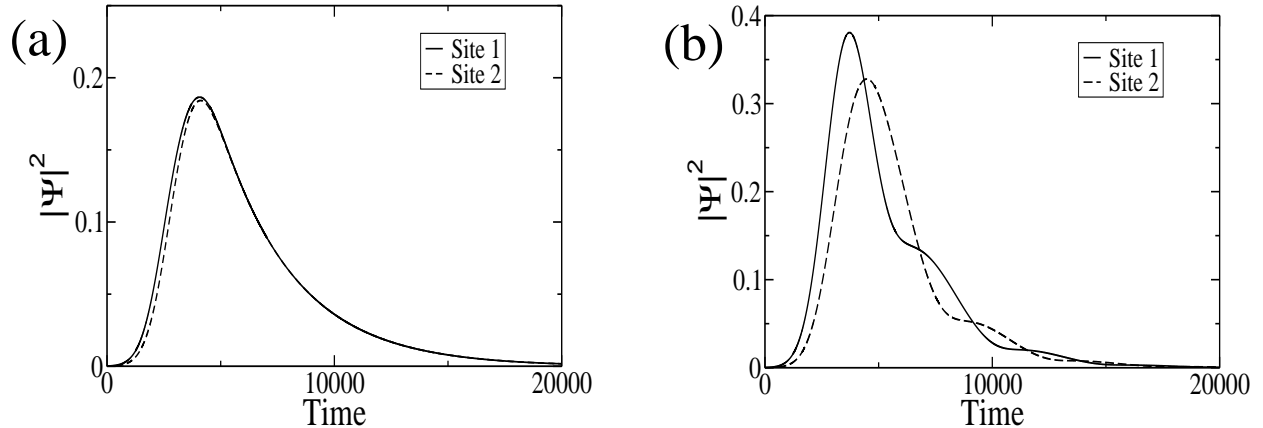


FIG. 11: Population of the ABL mode (a) and of the CM mode (b) on the two different sites that are connected to the vibration as a function of time (atomic units). The ABL mode shows the same population for the two sites as a function of time, while the CM mode presents a time dependent sequential population.

without any time dependence (except the one due to the coupling to the electrodes that we have neglected in this simplified discussion) because  $\psi_\sigma$  is basically an eigenstate of the Hamiltonian. This explains Fig. 11 (a).

In the case of the CM mode, we saw above that a single-site analogy cannot be applied and we have the two molecular orbitals involved in the wave packet propagation. Let us again approximate the wave packet by the evolution on the two sites:

$$|\Psi(t)_{\text{CM}}|^2 \approx |\psi_{\sigma^*}|^2 + |\psi_\sigma|^2 + 2\text{Re}(\psi_{\sigma^*}^* \psi_\sigma e^{i(\varepsilon_{\sigma^*} - \varepsilon_\sigma)t})$$

where a clear time dependence subsists. In good agreement with Fig. 11 (b).

## B. Two-sites and two vibrations

When more than one phonon per mode is needed to be converged with respect to the electron-vibration coupling, the inelastic transmission cannot be separated in additive contributions from different modes and all of them have to be considered at the same time.



A simple explanation for the increase of conductance in the tunneling regime was already advanced in IETS of metal-insulator-metal junctions<sup>44</sup>. The conductance increases because new conduction channels become available above a vibrational threshold. This interpretation is correct when the vibrational side bands of the electron transmission lie beyond  $\hbar\Omega$  of the electrode's Fermi energy. As we have already seen, opening a new channel means that we have to add the  $n = 1$  contribution to the  $n = 0$  contribution of the transmission. Hence, the  $\mathcal{Z}$  will present a positive peak at positive voltage, and negative at negative voltage<sup>44</sup>.

However, we can also have decreases of conductance. This is experimentally found in tunneling<sup>62</sup> and in contact regimes<sup>12</sup>. In the present theory, one always adds a positive contribution to the transmission above the vibrational threshold, but the change in conductance is given by the slope of the transmission, and this can have a rapid variation in the presence of a sideband. In the case where the sideband is in the tail of the main peak, and the width of the main peak is in the order of the vibrational frequency, then the slope will change from a smoothly varying one to the faster varying sideband slope, giving rise to a negative  $\mathcal{Z}$  at positive voltage. Let us give two examples of the above cases.

### A. Tunneling regime

In the case of the excitation of the CO frustrated rotation mode<sup>63</sup>, the  $2\pi^*$  and the  $5\sigma$  molecular orbitals are coupled via the electron-vibration coupling. This is easily seen by symmetry arguments<sup>64</sup>, since the mode is antisymmetric with respect to the planes containing the molecular axis and the non-zero matrix elements will couple a symmetric orbital ( $5\sigma$ ) with an antisymmetric one (the  $2\pi^*$ )<sup>65</sup>. Assuming weak coupling, we can neglect the effect of all other modes and estimate the change in conductance by using the two-site model coupled to a vibration that we presented above. Figure 12 shows the result of the conductance, Eq. (10), and in the corresponding  $\mathcal{Z}$ . We see that the Fermi energy plus  $\Omega$  for the frustrated rotation, gives the threshold where the transmission for  $n = 1$  enters, giving a clear discontinuity in the conductance (positive contribution) and hence a positive peak in the  $\mathcal{Z}$ . This is the case in metal-insulator-metal junctions<sup>44</sup>. The two-level model leads to different inelastic efficiencies at positive and negative voltage bias.

However, the case of IETS of  $\text{O}_2$  on  $\text{Ag}(110)$ <sup>62</sup> is different. Experimentally, dips are found instead of positive peaks in the  $\mathcal{Z}$ . Let us consider the excitation of the internal stretch mode.

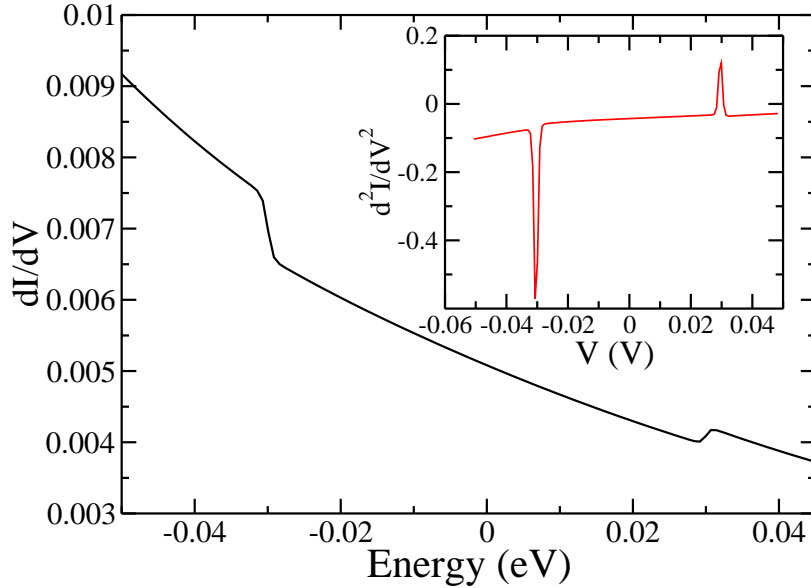


FIG. 12: Conductance for a model system of two levels of CO on Cu(100). In the inset the  $\mathcal{Z}$  is depicted. The asymmetry in the size of the change in conductance is a consequence of the two-level model. The variation in the conductance away from the vibrational threshold is due to the energy dependence of the two-level density of states. As can be seen in the  $\mathcal{Z}$ , the variation is small with respect to the inelastic change in conductance.

By computing the PDOS on molecular orbitals<sup>66</sup>, we know that the  $\pi_g$  perpendicular to the surface is close to the Fermi energy, and that tunneling takes place through it<sup>66</sup>. The mode has the same symmetry as the molecular orbital and the diagonal matrix element will be different from zero. We are hence in a case that can be approximated by the single-site model. Figure 13 shows the result. We have located the  $\pi_g$  at the Fermi energy as the PDOS on molecular orbitals<sup>66</sup> seems to indicate. The orbital width is taken as 0.1 eV and the frequency energy is 0.08 eV. We see that the transmission function is an asymmetric peak because the sideband is inserted in the tail of the main peak. We also include the contribution of  $n = 1$  above the Fermi energy plus the frequency in order to calculate the  $\mathcal{Z}$ , as for the CO case while we prefer to plot the complete one-electron transmission because in the present case the initial level occupation matters and we cannot treat it in this one-electron approach. Instead, we realize that we see the change of slope due to the side bands in the  $n = 0$  and  $n = 1$  contributions. The  $\mathcal{Z}$  gives a dip corresponding to the change of slope of the  $n = 0$  contribution. Hence, the elastic component of the transmission contains the

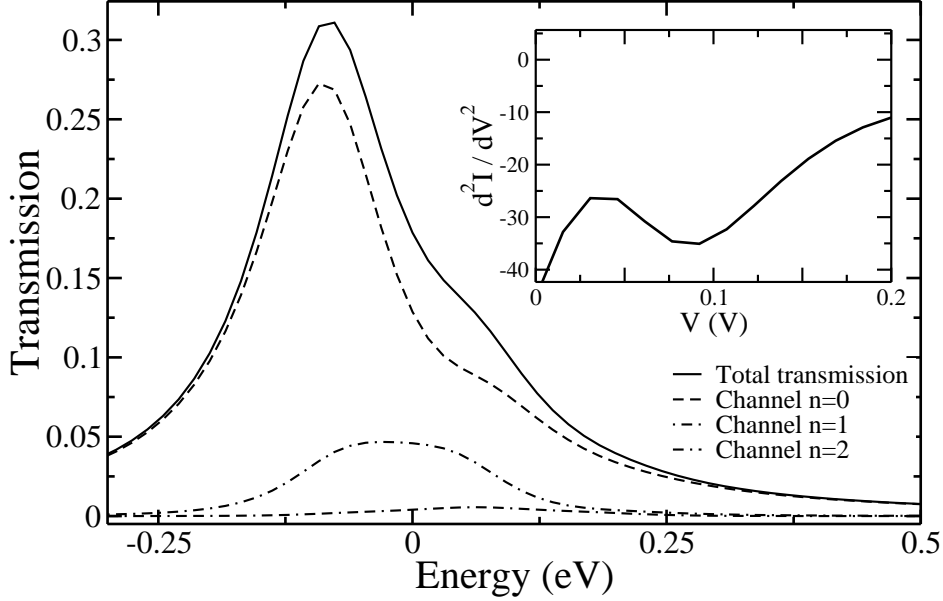


FIG. 13: Transmission for a model system of two levels of  $O_2$  on Ag (110). In the inset the  $\mathcal{Z}$  is depicted. The decrease in the  $\mathcal{Z}$  originates in the change of slope of the transmission due to the vibrational side bands. These side bands belong to all vibrational channels, in particular to the elastic one. Hence, the contribution of the elastic channel alone gives a decrease in conductance because the density of states is rapidly changing due to the electron-vibration coupling.

information of the IETS. The decrease of conductance in this case is due to the rapid change of transmission already in the elastic channel. It is then a decrease due to the variation of the vibronic density of states.

From these models we conclude that negative peaks in the  $\mathcal{Z}$  are due to sidebands in the elastic transmission. This statement is equivalent to the one found in the pioneering work by Davis<sup>67</sup>. Davis realized that a decrease of conductance could be found in some especial circumstances. Namely, that the single-site resonance was at the Fermi energy and that the resonance width was of the order of the vibrational frequency. These are the same conditions as we find. The interpretation by Davis is that virtual phonons were emitted and absorbed giving rise to an interference pattern. This interpretation is based on perturbation theory, and it just accounts for the vibration's effect on the elastic channel. In our terms, it is just the vibrational sideband of the elastic channel. The only cases in which a vibrational sideband can yield a decrease in conductance is when the main peak of the transmission is at the Fermi energy<sup>68</sup> (this is half-filling, we discuss below that we cannot have half-filling

in our models), and the electronic widths are of the order than the vibrational frequency, so as to enlarged and distort the main peak by the sideband. In the case of half-filling, the sidebands are symmetric with respect to the Fermi energy<sup>30</sup> giving rise to a peak at negative voltage and to a dip at positive one in the  $\mathcal{I}$ . The voltage of the dip does not exactly correspond to the vibrational frequency, since it correspond to the largest slope of the vibrational side band, not its maximum. Hence, these results suggest that the voltages at the dips are not direct measurements of the vibrational frequencies, while in the case of the voltages corresponding to peaks in the  $\mathcal{I}$ , are direct readings of the vibrational frequencies.

There is certain confusion in the literature because perturbation theory is currently used. In this case the current in the absence of electron-phonon coupling is confused with the elastic current. As can be seen in Fig. 3 (a) in the absence of electron-phonon coupling one gets a single lorentzian peak (dashed lines), however the elastic contribution is the  $n = 0$  curve of Fig. 3 (b). Hence, it is wrong to identify the elastic current with the one without electron-vibration coupling.

## B. Contact regime

Paulsson and co-workers<sup>69</sup> have shown that in the case of symmetric contact to the electrodes one can continuously pass from a peak to a dip in the  $\mathcal{I}$  by increasing the transmission probability. At transmission  $1/2$  the threshold between both behaviors is found. In the case of contact, a large density of states is pinned at the Fermi energy. Hence, it is  $\Gamma$  the parameter that controls the coupling to the leads and, therefore, the passage from peaks to dips in the change of conductance at the vibration threshold. Recent experimental evidence has been reported in 70.

Figure 14 shows the behavior of the electronic wave packet after collision with a 4-site chain in the contact regime. The parameters are those from Ref. 71. The chosen mode is the ABL, that corresponds to the one giving the largest change in conductance in gold monoatomic chains<sup>12</sup>. The wave packet is mainly transmitted in the elastic channel as is to be expected from the contact regime, however the vibrationally excited wave packets are mainly reflected in agreement with the interpretation of Ref. 12. However, the behavior is more complex: electronic wave packets in channels with odd  $n$  are reflected, even  $n$  are transmitted. In this particular calculation, the reflection of the  $n = 1$  component is due to

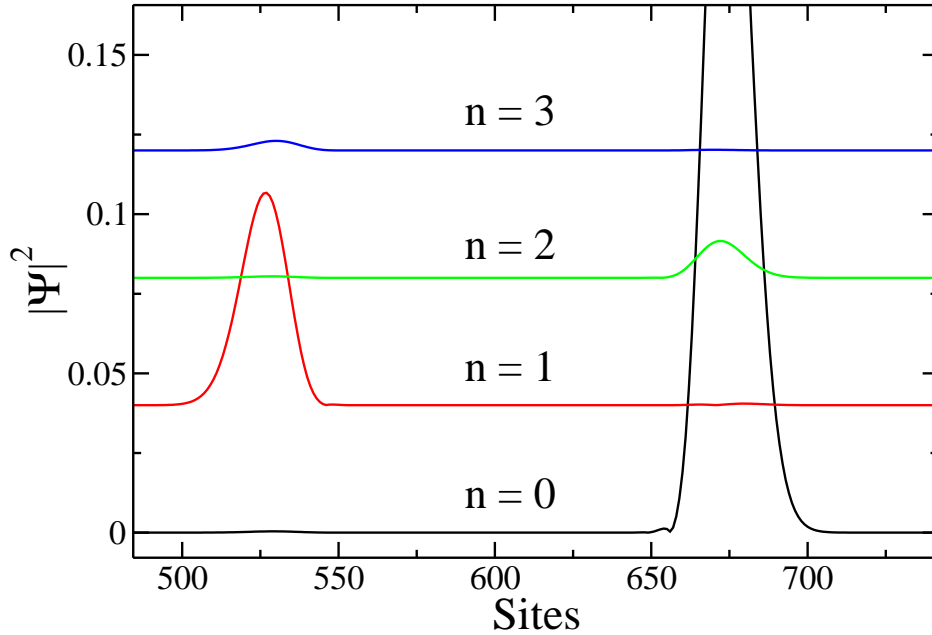


FIG. 14: (Color online) Electronic wave packets for different vibrational channels at a time instance after the elastic wave packet has passed the vibrating chain centered at site 600. Four electronic sites are connected to an ABL vibration. This 4-site chain is strongly coupled to the leads, representing the contact regime. Hence, the elastic wave packet is basically unperturbed by the chain, but the vibrationally excited channels have wave packets that are reflected for odd  $n$ , and transmitted for even  $n$ .

finite-band effects. As we discussed above, a finite band leads to the closing of transmission channels when inelastic effects are operative, increasing the electronic wave packet reflection. As the number of vibrational excitations increases, the closing of channels corresponds to each excitation process, implying an increase of the reflection in each case. As a consequence, even excitations mean even number of reflections, leading to an increase in transmission. Indeed, we have found this behavior for large transmission even in the single-site case.

Some of the calculations of Ref. 69 have been performed in the wide-band approximation, and hence the closing of channels due to finite-band effects is not present. Hence, we cannot conclude that the decrease in conductance leads to an increase in electron reflection such as the one found in this section. Instead, we think their calculations correspond to the regime where rapid changes in the vibronic density of states are found which correspond to the precedent section.

## VII. MANY-ELECTRON AND ELECTRON-ELECTRON EFFECTS IN THE PRESENCE OF VIBRATIONS

Our calculations are exact regarding the vibrational dynamics during electron transport. The price to pay is the neglect of multielectron effects. The description of multielectron effects together with vibrational excitation necessarily implies approximations. A recent treatment of both effects is the one by Galperin et al.<sup>20</sup>. Despite approximations, their treatment is correctly evaluating the vibrational dynamics. Indeed, we can reproduce their results, and the main difference between both calculations is an absorption shoulder appearing below the first peak in the multielectron case. According to Ref. 20 this is due to the propagation of holes coexisting with electron transport. This is absent in our one-electron treatment.

Even in the absence of a direct electron-electron interaction in the Fröhlich-Holstein model used here, Eq. (6), the electron-vibration coupling can lead to effective electron-electron interactions, see for example Ref. 30. This leads to electron-electron correlations and has extensively been studied in the literature in the so-called bi-polaron problem<sup>72</sup>. This is absent in our one-electron approach, but could in principle be treated by using two-electron propagations.

Perhaps, more important for the description of transport in metallic systems is the absence of the initial electron occupation in the present approach. This is easily solved by usual non-equilibrium Green's functions approaches<sup>30</sup> at the price of simplifying the treatment on the phononic description. Indeed, while the present approach treats the nuclear-coordinate description exactly within the one-electron problem and the harmonic approximation, NEGF approaches need to rely on approximate treatments<sup>20,30,32</sup>. This situation can be solved by using a time-dependent Hartree-Fock approach to generate a many-body wave packet, extending the present treatment to a multielectron case. Some encouraging results in time-dependent Hartree-Fock and beyond techniques have been presented in Refs. 73,74.

## VIII. SUMMARY AND CONCLUSIONS

Time-dependent wave packet propagations for the study of inelastic effects in electron transport can be very interesting because of the physical picture they permit us to de-

velop as well as the good size-scaling properties that they can have. Indeed, in the case of sparse Hamiltonians, the scaling is basically linear with the system size, when Lanczos-like propagation methods are used.

In the present work we have analyzed the electron-vibration problem when a single electronic site is connected to two electrodes. We have used a time-dependent description to understand the vibrational excitation sequence, the electronic phase shift and the interference patterns. The time-dependent calculation has given us access to the same quantities we can calculate using an energy-resolved theory, but with the time-dependent insight.

We have also studied the case of two sites and two vibrational modes, and we have realized that the two-site problem can be simplified to the single-site one when molecular orbitals can be used. The electron-vibration coupling will determine when molecular orbitals are meaningful. This is seen by changing the electron-vibration coupling matrix to the molecular-orbital basis set. Pursuing this idea, we have developed a simple hybridisation scheme that permits us to understand the vibronic structure of an electron transmission function in terms of the symmetry of the electron-vibration couplings. We have shown, that for medium and strong electron-vibration coupling all modes need to be considered.

We have applied our simple model to get some insight in the case of the vibrational excitation of CO on Cu(100)<sup>63</sup> and O<sub>2</sub> on Ag(110)<sup>62</sup>. Due to our one-electron treatment, the calculations are missing fundamental ingredients, but they permit us to explain the IETS signals in terms of vibrational channels. In the case of O<sub>2</sub>, the calculation show that the elastic channel leads to a decrease in the  $\mathcal{Z}$ . Contrary to perturbation theory, the elastic channel is not the electronic structure in the absence of electron-vibration coupling, but the  $n = 0$  transmission function. Hence the elastic channel contains all of the information about the electron-vibration coupling. In particular, the elastic contribution will contain vibrational satellites. These satellites or side bands have a strong energy dependence that naturally leads to dips in the  $\mathcal{Z}$ . Indeed this means that the density of states that should be considered is the vibronic one, this density of states contain rapid variations with the energy that lead to decreases of  $\mathcal{Z}$ . In perturbation theory, one needs to consider the effect of the vibration in the elastic channel to retrieve the effect of the vibration in the electronic structure and hence to take into account the vibronic density of states in the conductance.

We have also explored the case of contact with the two electrodes. In this case, it has been shown that the conductance should drop at the vibrational thresholds because

the vibrations backscatter the impinging electrons. Our calculation show that for the first excited (and generally odd vibration channel,  $n$ ) the electronic wave packet is reflected at the vibration. However for even  $n$  the wave packet is transmitted. This behavior is due to the finite electronic band of the present calculation, that leads to the closing of inelastic channels increasing reflection. An even number of consecutive reflections lead to increased transmission.

New developments in time-dependent Hartree-Fock lead us to think that a full time-dependent treatment of the physics usually explored with non-equilibrium Green's functions will be soon available permitting us to develop a different point of view on inelastic effects in electron transport on the atomic scale.

### Acknowledgments

Interesting discussions with A. Arnau, A.-G. Borisov, T. Frederiksen, J.-P. Gauyacq, E. Jeckelmann, T. Klamroth, M. Paulsson, P. Saalfrank, and H. Ueba are gratefully acknowledged. N.L. acknowledges support from the Spanish MEC (No. FIS2006-12117-C04-01). Computer resources of the Centre de Calcul de Midi-Pyr nee (CALMIP) are gratefully acknowledged.

- 
- <sup>1</sup> M. Galperin, M. A. Ratner, A. Nitzan, and A. Troisi, *Science* **319**, 1056 (2008).
  - <sup>2</sup> M. Galperin, M. A. Ratner, A. Nitzan, *J. Phys.: Cond. Matter* **19**, 103201 (2007).
  - <sup>3</sup> M. Berthe, A. Urbieto, L. Perdigo, B. Grandidier, D. Deresmes, C. Delerue, D. Stievenard, R. Rurali, N. Lorente, L. Magaud, P. Ordejon, *Phys. Rev. Lett.* **97**, 206801 (2006).
  - <sup>4</sup> N. N el, J. Kr ger, L. Limot, T. Frederiksen, M. Brandbyge, and R. Berndt, *Phys. Rev. Lett.* **98**, 065502 (2007).
  - <sup>5</sup> W. Ho, *J. Chem. Phys.* **117**, 11033 (2002).
  - <sup>6</sup> B. C. Stipe, M. A. Rezaei, W. Ho, *Science* **279**, 1907 (1998).
  - <sup>7</sup> H. J. Lee and W. Ho, *Science* **286**, 1719 (1999).
  - <sup>8</sup> J. Gaudioso, L. J. Lauhon, W. Ho, *Phys. Rev. Lett.* **85**, 1918 (2000).
  - <sup>9</sup> Y. Kim, T. Komeda and M. Kawai, *Phys. Rev. Lett.* **89**, 126104 (2002).

- <sup>10</sup> X. H. Qiu, G.V. Nazin and W. Ho, *Science* **299**, 542 (2003).
- <sup>11</sup> R. H. Smit, Y. Noat, C. Untiedt, N. D. Lang, M. C. V. Hermet, and J. M. V. Ruitenbeek, *Nature* **419**, 906 (2002).
- <sup>12</sup> N. Agrait, C. Untiedt, G. Rubio-Bollinger, S. Vieira, *Phys. Rev. Lett.* **88**, 216803 (2002).
- <sup>13</sup> N. Mingo and K. Makoshi, *Surf. Sci.* **438**, 261 (1999); *Phys. Rev. Lett.* **84**, 3694 (2000).
- <sup>14</sup> N. Lorente and M. Persson, *Phys. Rev. Lett.* **85**, 2997 (2000).
- <sup>15</sup> T. Mii, S. Tikhodeev, and H. Ueba, *Surf. Sci.* **502**, 26 (2002); *Phys. Rev. B* **68**, 205406 (2003).
- <sup>16</sup> M. J. Montgomery, T. N. Todorov, *J. Phys.: Cond. Matt.* **15**, 8781 (2003).
- <sup>17</sup> T. Frederiksen, M. Brandbyge, N. Lorente and A.-P. Jauho, *Phys. Rev. Lett.* **93**, 256601 (2004).
- <sup>18</sup> G. C. Solomon, A. Gagliardi, A. Pecchia, T. Frauenheim, A. Di Carlo, J. R. Reimers, N. S. Hush, *J. Chem. Phys.* **124**, 094704 (2006).
- <sup>19</sup> M. Galperin, M. A. Ratner, A. Nitzan, *J. Chem. Phys.* **121**, 11965 (2004).
- <sup>20</sup> M. Galperin, A. Nitzan, M. A. Ratner, *Phys. Rev. B* **73**, 045314 (2006).
- <sup>21</sup> M. Paulsson, T. Frederiksen, M. Brandbyge, *Nano Letters* **6**, 258 (2006).
- <sup>22</sup> A. Troisi, M. A. Ratner, and A. Nitzan, *J. Chem. Phys.* **118**, 6072 (2003).
- <sup>23</sup> E. Prodan and R. Car, *Phys. Rev. B* **76**, 115102 (2007).
- <sup>24</sup> C. Verdozzi, G. Stefanucci and C.-O. Almbladh, *Phys. Rev. Lett.* **97**, 046603 (2006).
- <sup>25</sup> M. Di Ventra and R. D'Agosta, *Phys. Rev. Lett.* **98**, 226403 (2007).
- <sup>26</sup> E. McEniry and T. Todorov, *J. Phys.: Cond. Matt.* **19**, 196201 (2007).
- <sup>27</sup> S. Mahapatra and N. Sathyamurthy, *J. Chem. Soc., Faraday Trans.*, **93**, 773 (1997).
- <sup>28</sup> J.-P. Gauyacq, *J. Chem. Phys.* **93**, 384 (1990).
- <sup>29</sup> A. Bringer, J. Harris and J. W. Gadzuk, *J. Phys.: Condens. Matter* **5**, 5141 (1993).
- <sup>30</sup> P. Hyldgaard, S. Hershfield, J. H. Davies and J. W. Wilkins, *Annals of Physics* **236**, 1 (1994).
- <sup>31</sup> K. Flensberg, *Phys. Rev. B* **68**, 205323 (2003).
- <sup>32</sup> A. Mitra, I. Aleiner and A. J. Millis, *Phys. Rev. B* **69**, 245302 (2004).
- <sup>33</sup> Y. Imry, O. Entin-Wohlman, and A. Aharony, *Europhys. Lett.* **72**, 263 (2005).
- <sup>34</sup> H. Ness, *J. Phys.: Condens. Matter* **18**, 6307 (2006).
- <sup>35</sup> T. Markussen, R. Rurali, M. Brandbyge, and A.-P. Jauho, *Phys. Rev. B* **74**, 245313 (2006).
- <sup>36</sup> S. Roche, J. Jiang, F. Triozon, R. Saito, *Phys. Rev. Lett.* **95**, 076803 (2005).
- <sup>37</sup> J.C. Lanczos, *J. Res. Natl. Bur. Stand.* **45**, 225 (1950).
- <sup>38</sup> J. K. Cullum, R.A. Willoughby, Lanczos algorithms for large eigenvalue computations, SIAM

- (2002).
- <sup>39</sup> A. G. Borisov, S. V. Shabanov, *J. Comput. Phys.* **209**, 643 (2005).
- <sup>40</sup> J. Sjakste, A. G. Borisov, J.-P. Gauyacq, A.K. Kazansky, *J. Phys. B* **37**, 1593 (2004).
- <sup>41</sup> D. J. Tannor, *Introduction to quantum mechanics: a time dependent perspective*, University Science, Sausalito (2006).
- <sup>42</sup> T. Holstein, *Ann. Phys. (NY)* **8**, 325 (1959).
- <sup>43</sup> Y. Meir, N. S. Wingreen, *Phys. Rev. Lett.* **68**, 2512 (1992).
- <sup>44</sup> P. K. Hansma, *Phys. Rep.* **30**, 145 (1977).
- <sup>45</sup> B. Y. Gelfand, S. Schmitt-Rink, and A. F. J. Levi, *Phys. Rev. Lett.* **62**, 1683 (1989).
- <sup>46</sup> J. A. Stovneng, E. H. Hauge, P. Lipavsky and V. Spicka, *Phys. Rev. B* **44**, 13595 (1991).
- <sup>47</sup> N. S. Wingreen, K. W. Jacobsen and J. W. Wilkins, *Phys. Rev. Lett.* **61**, 1396 (1988); *Phys. Rev. B* **40**, 11834 (1989).
- <sup>48</sup> J. W. Gadzuk, *Phys. Rev. B* **44**, 13466 (1991).
- <sup>49</sup> J. Bonca, S. A. Trugman, *Phys. Rev. Lett.* **75**, 2566 (1995).
- <sup>50</sup> E. G. Emberly and G. Kirczenow, *Phys. Rev. B* **61**, 5740 (2000).
- <sup>51</sup> M. Cizek, M. Thoss and W. Domcke, *Phys. Rev. B* **70**, 125406 (2004).
- <sup>52</sup> Ph. Durand, I. Páidarová and F.-X. Gadea, *J. Phys. B: At. Mol. Opt. Phys.* **34**, 1953 (2001).
- <sup>53</sup> A. Baratoff and B. N. J. Persson, *J. Vac. Sci. Tech.* **6**, 331 (1988).
- <sup>54</sup> J.-P. Gauyacq, *Dynamics of negative ions*, World Scientific Lecture Notes in Physics, Singapore (1987).
- <sup>55</sup> M. Persson and B. Hellsing, *Phys. Rev. Lett.* **49**, 662 (1982); B. Hellsing and M. Persson, *Phys. Scr.* **29**, 360 (1984).
- <sup>56</sup> We assume that the main difference between the negative PES and the neutral one is the change in geometrical conformation of the negative ion with respect to the neutral molecule. However, frequencies also change and as a matter of fact the electron-vibration coupling should be computed for the negative PES.
- <sup>57</sup> J. Repp, G. Meyer, S. Paavilainen, F. E. Olsson and M. Persson, *Phys. Rev. Lett.* **95**, 225503 (2005).
- <sup>58</sup> G. D. Mahan, *Many-particle physics*, Kluwer Academic/Plenum Publishers, 3<sup>rd</sup> Ed., New York (2000), p. 226.
- <sup>59</sup> T. Frederiksen, N. Lorente, M. Paulsson, M. Brandbyge, *Phys. Rev. B* **75**, 235441 (2007).

- <sup>60</sup> N. A. Pradhan, N. Liu and W. Ho, *J. Phys. Chem. B* **109**, 8513 (2005).
- <sup>61</sup> N. Ogawa, G. Mikaelian and W. Ho, *Phys. Rev. Lett.* **98**, 166103 (2007).
- <sup>62</sup> J. R. Hahn, H. J. Lee and W. Ho, *Phys. Rev. Lett.* **85**, 1914 (2000).
- <sup>63</sup> L. J. Lauhon and W. Ho, *Phys. Rev. B* **60**, R8525 (1999).
- <sup>64</sup> N. Lorente, R. Rurali and H. Tang, *J. Phys.: Condens. Matt.* **17**, S1049 (2005).
- <sup>65</sup> N. Lorente and M. Persson, *Faraday Discussions* **117**, 277 (2000).
- <sup>66</sup> F. E. Olsson, N. Lorente and M. Persson, *Surf. Sci.* **522**, L27 (2003).
- <sup>67</sup> L. C. Davis, *Phys. Rev. B* **2**, 1714 (1970).
- <sup>68</sup> B. N. J. Persson and A. Baratoff, *Phys. Rev. Lett.* **59**, 339 (1987).
- <sup>69</sup> M. Paulsson, T. Frederiksen, and M. Brandbyge, *Phys. Rev. B* **72**, 201101(R) (2005).
- <sup>70</sup> O. Tal, M. Krieger, B. Leering, and J. M. van Ruitenbeek, *cond-matt.mes-hal* arXiv:0801.3031v1
- <sup>71</sup> T. Frederiksen, M. Brandbyge, A. P. Jauho, N. Lorente, *J. Comp. Elec.* **3**, 423 (2004).
- <sup>72</sup> C. Zhang, E. Jeckelmann and S. R. White, *Phys. Rev. Lett.* **80**, 2661 (1998); *Phys. Rev. B* **69**, 14092 (1999).
- <sup>73</sup> M. Nest and T. Klamroth, *Phys. Rev. A* **72**, 012710 (2005).
- <sup>74</sup> P. Krause, T. Klamroth, and P. Saalfrank, *J. Chem. Phys.* **127**, 034107 (2007).